Journal of
Mechanics of
Materials and Structures

A MODIFIED SHEAR-LAG MODEL FOR PREDICTION OF
STRESS DISTRIBUTION IN UNIDIRECTIONAL FIBROUS COMPOSITES
CONSIDERING INTERPHASE

Mohammad Hassan Zare and Mehdi Mondali

msp

■
■
■msp

A MODIFIED SHEAR-LAG MODEL FOR PREDICTION OF
STRESS DISTRIBUTION IN UNIDIRECTIONAL FIBROUS COMPOSITES
CONSIDERING INTERPHASE

MOHAMMAD HASSAN ZARE AND MEHDI MONDALI

A modified shear-lag model is developed for unidirectional fibrous composites by considering the interphase region subjected to axial loading. A perfect bond at the fiber/interphase and interphase/matrix interfaces is assumed. The fiber, interphase, and matrix materials behave elastically during the analysis. The axial and shear stresses in fiber, interphase and matrix are analytically obtained as functions of the radial and axial directions using a micromechanical approach in a full-continuum model. The composite axial displacement and composite elastic modulus also are obtained. In order to consider the effect of inhomogeneity of the interphase in the three-phase micromechanics model, the elastic modulus of the interphase is assumed to vary with the radial coordinate. Two case studies, a carbon nanotube-reinforced polymer composite and an aramid fiber-reinforced rubber composite are used to validate the results of the model. The results predicted by the proposed analytical approach exhibited good agreement with the finite element results and available experimental measurements.

1. Introduction

The mechanical properties of composite materials are affected by geometrical factors and the structural behavior of the composite constituents [Fu et al. 2008; Lauke 2006]. In many composites reinforced by continuous or discontinuous fibers, there is also an interphase region which transmits the load between the matrix and fiber like a bridge. The interphase is an important constituent with significant effects on the performance of fiber-reinforced composites [Yang and Pitchumani 2004]. One concern during the modeling of the interphase region is its dimensional specifications and physical properties, which can be provided through experimental methods. Typical examples of composite materials having interphase regions are polymer composites reinforced with carbon nanotubes (CNTs) and hybrid fiber-reinforced rubber composites.

Several numerical studies have been conducted to investigate the effects of interphase mechanical properties on stress transfer of fiber-reinforced composites [Maligno et al. 2010; Wang et al. 2006; 2011]. Because of the importance of and wide applications for nanocomposites, numerical modeling using full-continuum or semicontinuum models has been the goal of many researchers. In full-continuum models, the material of the interphase region behaves as a continuum with constant or variable mechanical properties. In semicontinuum models, the interphase region consists of a regular set of spring elements which make the modeling and solution complicated and time-consuming [Wan et al. 2005; Needleman et al. 2010; Hernández-Pérez and Avilés 2010; Golestanian and Shojaie 2010; Kumar and Srinivas 2014; Rafiee and Pourazizi 2015]. Kumar and Srinivas [2014] used a three-phase finite element (FE) model to

analyze the effect of interphase properties on the elastic modulus of nanocomposites. The effect of CNT functionalization on the properties of interphase regions has been studied by Rafiee and Pourazizi [2015]. In their model, the interaction between CNTs and polymer in the interphase region was simulated using the semicontinuum approach.

Analytical methods can also be used to consider the effect of the interphase region in a unit cell. However, the complexity of the solution has meant that analytical studies have primarily been carried out without considering the interphase region [Muki and Sternberg 1970; Lawrence 1972; Takaku and Arridge 1973; Luk and Keer 1979; Budiansky et al. 1986; Kerans and Parthasarathy 1991; Abedian et al. 2007; Gao and Li 2005; Haque and Ramasetty 2005; Ang and Ahmed 2013]. The most well-known analytical model for describing the load transfer mechanism from matrix to reinforcement in fibrous composites is the shear-lag model presented by Cox [1952] and subsequently modified by others [Dow 1963; Rosen 1964; Nair and Kim 1992; Hsueh 1995]. In this theory, the load applied to the matrix is transferred to reinforcements through its cylindrical walls.

In comparison with models such as those by Tsai [Halpin 1984] and Eshelby [Taya and Arsenault 1987; Withers et al. 1989], the shear-lag model more comprehensively describes the load transfer mechanism from matrix to reinforcement; thus, researchers have tried to overcome the shortcomings of this model [Gao and Li 2005; Ang and Ahmed 2013; Nairn 1997; Zhao and Ji 1997; Beyerlein and Landis 1999; Zhang and He 2008]. Studies have also been conducted stress analysis of fibrous composites based on elasticity theory. Abedian et al. [2007] presented a micromechanics model to determine the elastic stress field in fiber-reinforced composites. In this model, the shear stress was obtained as a function of both radial and axial directions using the exact solution of the displacement fields in the matrix and reinforcement.

One shortcoming of the shear-lag model is its inability to consider the interphase region, but consideration of this region is required for improving the accuracy of analysis. Yao et al. [2013] investigated the effect of a graded interphase on the mechanism of stress transfer in a fiber reinforced composite using an improved shear-lag model with simple assumptions. The inhomogeneity of the interphase in their model was represented by the graded feature of the Young's modulus, which is graded according to a power law or a linear law in the radius direction.

Researchers have recently used the shear-lag model for CNT-reinforced polymer composites and hybrid fiber-reinforced rubber composites using the representative volume element [Gao and Li 2005; Haque and Ramasetty 2005; Liu and Chen 2003; Zhang et al. 2017]. Gao and Li [2005] developed a two-phase shear-lag model for CNT-reinforced polymer composites using a multiscale approach. Haque and Ramasetty [2005] analyzed a two-phase continuous fiber model of CNT-reinforced polymer composites to predict the interfacial axial and shear stresses.

The interface properties of CNT-reinforced composites were determined by Ang and Ahmed [2013] using an improved shear-lag model. The analytical results obtained by Ang and Ahmed were used to investigate the stress sustainability of CNT-reinforced polymer composites. Recently, a shear-lag model for stress analysis in hybrid fiber-reinforced rubber composites was presented by Zhang et al. [2017]; however, the model cannot determine the radial dependence of shear and axial stresses in the fiber and matrix.

The present study micromechanically analyzed unidirectional fibrous composites by considering the interphase region using a new modified shear-lag model. All stress components, including the shear and

axial stresses, in the fiber, interphase and matrix have been analytically obtained as functions of both the radial and axial directions. In order to consider the effect of inhomogeneity of the interphase, it was assumed that interphase properties such as elastic modulus will vary with the variation of the unit cell radius. To validate the results of the proposed model, two case studies on CNT-reinforced polymer composites and aramid fiber-reinforced rubber composites are presented to provide practical applications for this model.

The proposed model can also be applied for stress analysis of short fiber composites considering the interphase, which has not been addressed by other researchers thus far. The imaginary fiber technique was chosen to analyze the stress field in short fiber composites. In this method, the unit cell is divided into two regions (I and II) along the model length [Abedian et al. 2007; Hsueh 1988; 1990; 1992; 2000; Hsueh et al. 1997; Mondali and Abedian 2013]. Region I consists of the fiber and matrix and region II is the matrix material. The stress field in region I is determined first. The relations obtained for the stress field in region I can be used in region II if the mechanical properties of the fiber are replaced by the mechanical properties of the matrix in these relations. In fact, because the matrix along the fiber in region II is an "imaginary" fiber, this technique is known as the imaginary fiber technique.

The relation constants can be determined using appropriate continuity conditions on the common boundary of regions I and II. The significant difference and novelty of the present study with respect to the state-of-the-art is its ability to carry out stress analysis on the short fiber composites with interphase regions. It is necessary to note that application of the present model to short fiber composites and development of a modified imaginary fiber technique is currently being undertaken and the related articles will be published in the future.

2. Analytical method

2.1. *RVE modeling.* Analysis of the three-phase micromechanics unit cell was carried out using a full-continuum model. A continuous cylindrical fiber with radius r_f and length of $2l_f$ is surrounded by an interphase region with radius r_{ip} and thickness t_i. The interphase region is homogeneously and isotropically located between matrix and fiber, see Figure 1 (left).

The cylindrical polar coordinate system (r, θ, z) was used with the origin at the center of the unit cell. Geometrical symmetry, loading, and boundary conditions meant that analysis of three-phase model RVE could be performed only on the half length of l_m outside radius r_m in a 2D axisymmetric model of the unit cell, see Figure 1 (right). The following assumptions were made for the purpose of analysis:
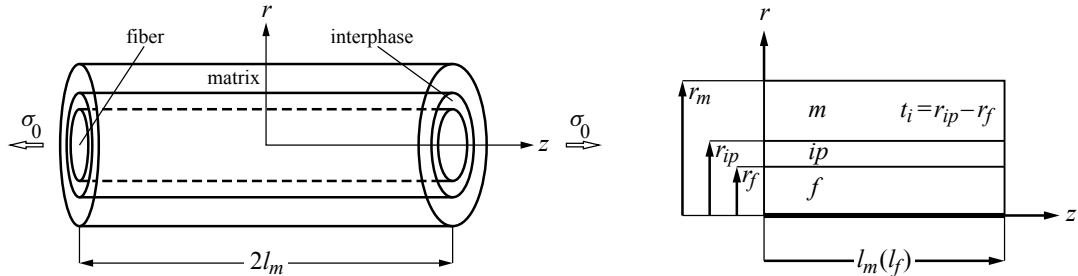
Figure 1. The three-phase model of RVE: 3D model (left) and 2D axisymmetric model (right).

(1) Interphase properties such as the elastic modulus vary with the unit cell radius.

(2) The fiber, matrix and interphase behave elastically.

(3) The analytical model is based on the shear-lag theory assuming a perfect bond at the fiber-interphase and interphase-matrix interfaces.

(4) Body and bonding forces are neglected in equilibrium equations.

(5) Partial derivatives of radial displacement relative to z are neglected [Gao and Li 2005; Yao et al. 2013].

2.2. *Governing equations and boundary conditions.* Governing equilibrium equations for axisymmetric problem in cylindrical coordinate are obtained as [Timoshenko and Goodier 1970]

$$\frac{\partial \sigma_{rr}^{\eta}}{\partial r} + \frac{\partial \tau_{rz}^{\eta}}{\partial z} + \frac{\sigma_{rr}^{\eta} - \sigma_{\theta\theta}^{\eta}}{r} = 0, \tag{1}$$

$$\frac{\partial \tau_{rz}^{\eta}}{\partial r} + \frac{\partial \sigma_{zz}^{\eta}}{\partial z} + \frac{\tau_{rz}^{\eta}}{r} = 0, \tag{2}$$

where superscript η is a variable that denotes the fiber, interphase, and matrix regions.

The constitutive equations of stress-strain for an isotropic material are

$$\varepsilon_{rr}^{\eta} = \frac{1}{E_{\eta}}[\sigma_{rr}^{\eta} - \nu_{\eta}(\sigma_{\theta\theta}^{\eta} + \sigma_{zz}^{\eta})], \tag{3}$$

$$\varepsilon_{\theta\theta}^{\eta} = \frac{1}{E_{\eta}}[\sigma_{\theta\theta}^{\eta} - \nu_{\eta}(\sigma_{rr}^{\eta} + \sigma_{zz}^{\eta})], \tag{4}$$

$$\varepsilon_{zz}^{\eta} = \frac{1}{E_{\eta}}[\sigma_{zz}^{\eta} - \nu_{\eta}(\sigma_{rr}^{\eta} + \sigma_{\theta\theta}^{\eta})], \tag{5}$$

$$\gamma_{rz}^{\eta} = \frac{\tau_{rz}^{\eta}}{G_{\eta}}. \tag{6}$$

Strain-displacement relations (geometrical equations) for axisymmetric problem are also given by

$$\varepsilon_{rr}^{\eta} = \frac{\partial u^{\eta}}{\partial r}, \tag{7}$$

$$\varepsilon_{\theta\theta}^{\eta} = \frac{u^{\eta}}{r}, \tag{8}$$

$$\varepsilon_{zz}^{\eta} = \frac{\partial w^{\eta}}{\partial z}, \tag{9}$$

$$\gamma_{rz}^{\eta} = \frac{\partial u^{\eta}}{\partial z} + \frac{\partial w^{\eta}}{\partial r}. \tag{10}$$

In the above relations, σ_{rr}^{η}, $\sigma_{\theta\theta}^{\eta}$, σ_{zz}^{η}, and τ_{rz}^{η} are the radial, circumferential, axial, and shear stresses, respectively. Also, ε_{rr}^{η}, $\varepsilon_{\theta\theta}^{\eta}$, ε_{zz}^{η}, and γ_{rz}^{η} are the radial, circumferential, axial, and shear strains components. Moreover, u^{η} and w^{η} are the radial and axial displacements and E_{η}, ν_{η}, and G_{η} are Young modulus, Poisson's ratio, and shear modulus of an isotropic material, respectively.

In such a problem, the applied boundary conditions are [Abedian et al. 2007]

$$\tau_{rz}^f(r_f) = \tau_{rz}^{ip}(r_f) = \tau_1, \tag{11}$$

$$\tau_{rz}^{ip}(r_{ip}) = \tau_{rz}^m(r_{ip}) = \tau_2, \tag{12}$$

$$\tau_{rz}^m(r_m) = 0, \tag{13}$$

$$\overline{\sigma_{zz}^m}(\pm l_m) = \sigma_0, \tag{14}$$

$$\sigma_{rr}^m(r_m) = 0, \tag{15}$$

$$\sigma_{rr}^f(r_f) = \sigma_{rr}^{ip}(r_f), \tag{16}$$

$$\sigma_{rr}^{ip}(r_{ip}) = \sigma_{rr}^m(r_{ip}). \tag{17}$$

2.3. *Obtaining the shear stresses in fiber, interphase, and matrix.* The shear-lag relation for fiber can be obtained by integration of equilibrium (2) with respect to r from 0 to r_f as [Gao and Li 2005]

$$\frac{\partial \overline{\sigma_{zz}^f}}{\partial z} = -\frac{2\tau_1}{r_f}, \tag{18}$$

where $\overline{\sigma_{zz}^f}$ is the average axial normal stress over the cross-section of the effective fiber and τ_1 is the fiber-interphase interface shear stress.

Because $\partial \sigma_{zz}^f / \partial z$ in (2) is a function of z, by applying (11), the fiber shear stress as a function of r can be obtained as [Abedian et al. 2007]

$$\tau_{rz}^f = \frac{r}{r_f} \tau_1. \tag{19}$$

Then the shear-lag relation of the interphase is obtained by integration of (2) with respect to r from r_f to r_{ip} as

$$\frac{\partial \overline{\sigma_{zz}^{ip}}}{\partial z} = -\frac{2}{(r_{ip}^2 - r_f^2)} (r_{ip}\tau_2 - r_f\tau_1), \tag{20}$$

where $\overline{\sigma_{zz}^{ip}}$ is the average axial normal stress over the cross-section of the interphase and τ_2 is the interphase-matrix interface shear stress.

Similarly taking into account that $\partial \sigma_{zz}^{ip} / \partial z$ in (2) is a function of z and applying (11) and (12), the interphase shear stress as a function of r can be obtained as

$$\tau_{rz}^{ip} = \frac{\tau_1 r_f (r_{ip}^2 - r^2) + \tau_2 r_{ip}(r^2 - r_f^2)}{r(r_{ip}^2 - r_f^2)}. \tag{21}$$

As stated, equations (12) and (13) can be used to obtain the matrix shear stress as a function of r as [Abedian et al. 2007]

$$\tau_{rz}^m = \frac{r_{ip}}{(r_m^2 - r_{ip}^2)} \left(\frac{r_m^2}{r} - r \right) \tau_2. \tag{22}$$

However, the interfacial shear stresses $\tau_1(z)$ and $\tau_2(z)$ in (19), (21), and (22) are still unknown functions of z. Therefore, substituting (22) into (6) and (10), and then integrating with respect to r from r_{ip}

to r_m will yield

$$\tau_2 = G_m \frac{(r_m^2 - r_{ip}^2)}{r_{ip}[r_m^2 \ln(r_m/r_{ip}) - \frac{1}{2}(r_m^2 - r_{ip}^2)]} (w_{r_m}^m - w_{r_{ip}}^m), \tag{23}$$

where $w_{r_{ip}}^m$ and $w_{r_m}^m$ are the matrix axial displacements at r_{ip} and r_m, respectively.

Also, by substituting (23) into (21) and then substituting the obtained equation into (6) and (10), τ_1 can be expressed by integrating with respect to r from r_f to r_{ip} as

$$\tau_1 = \frac{G_{ip}(r_{ip}^2 - r_f^2)}{r_f[r_{ip}^2 \ln(r_{ip}/r_f) - \frac{1}{2}(r_{ip}^2 - r_f^2)]} (w_{r_{ip}}^{ip} - w_{r_f}^{ip})$$
$$+ \left[\frac{G_m[r_f^2 \ln(r_{ip}/r_f) - \frac{1}{2}(r_{ip}^2 - r_f^2)]}{[r_m^2 \ln(r_m/r_{ip}) - \frac{1}{2}(r_m^2 - r_{ip}^2)]} \times \frac{(r_m^2 - r_{ip}^2)(w_{r_m}^m - w_{r_{ip}}^m)}{r_f[r_{ip}^2 \ln(r_{ip}/r_f) - \frac{1}{2}(r_{ip}^2 - r_f^2)]} \right], \tag{24}$$

where $w_{r_f}^{ip}$ and $w_{r_{ip}}^{ip}$ are the interphase axial displacements at r_f and r_{ip}, respectively.

In this case, the terms $\partial u^\eta / \partial z$ for the matrix and interphase are neglected according to the assumption that $\partial u^\eta / \partial z \ll \partial w^\eta / \partial r$, which is reasonable because of the tensile loading condition and the symmetry of the model.

Finally, substituting (23) into (22) gives the matrix shear stress as

$$\tau_{rz}^m = G_m \frac{(w_{r_m}^m - w_{r_{ip}}^m)}{[r_m^2 \ln(r_m/r_{ip}) - \frac{1}{2}(r_m^2 - r_{ip}^2)]} \left(\frac{r_m^2}{r} - r \right). \tag{25}$$

Also, substituting (23) and (24) into (21) gives the interphase shear stress as

$$\tau_{rz}^{ip} = \left(\frac{r_{ip}^2}{r} - r \right) [A(w_{r_{ip}}^{ip} - w_{r_f}^{ip}) + B(w_{r_m}^m - w_{r_{ip}}^m)] + C \left(r - \frac{r_f^2}{r} \right)(w_{r_m}^m - w_{r_{ip}}^m), \tag{26}$$

where the constants A, B, and C are given as

$$A = \frac{G_{ip}}{\left(r_{ip}^2 \ln(r_{ip}/r_f) - \frac{1}{2}(r_{ip}^2 - r_f^2)\right)},$$
$$B = \frac{G_m(r_m^2 - r_{ip}^2)\left(r_f^2 \ln(r_{ip}/r_f) - \frac{1}{2}(r_{ip}^2 - r_f^2)\right)}{(r_{ip}^2 - r_f^2)\left(r_{ip}^2 \ln(r_{ip}/r_f) - \frac{1}{2}(r_{ip}^2 - r_f^2)\right)\left(r_m^2 \ln(r_m/r_{ip}) - \frac{1}{2}(r_m^2 - r_{ip}^2)\right)}, \tag{27}$$
$$C = \frac{G_m(r_m^2 - r_{ip}^2)}{(r_{ip}^2 - r_f^2)\left(r_m^2 \ln(r_m/r_{ip}) - \frac{1}{2}(r_m^2 - r_{ip}^2)\right)}.$$

2.4. *Obtaining the axial stresses in matrix and interphase.* In this section, $w^m(r, z)$, the matrix axial displacement, is determined first. Substituting (25) into (6) and (10), and then integrating with respect to r from r_{ip} to r will yield

$$w^m(r, z) = w_{r_{ip}}^m + \frac{r_m^2 \ln(r/r_{ip}) - \frac{1}{2}(r^2 - r_{ip}^2)}{\left(r_m^2 \ln(r_m/r_{ip}) - \frac{1}{2}(r_m^2 - r_{ip}^2)\right)} (w_{r_m}^m - w_{r_{ip}}^m). \tag{28}$$

Next, assuming that the radial and circumferential stresses in the matrix are much smaller than the axial stress $[(\sigma_{rr}^{\eta} + \sigma_{\theta\theta}^{\eta}) \ll \sigma_{zz}^{\eta}]$, one can neglect the term $(\sigma_{rr}^{\eta} + \sigma_{\theta\theta}^{\eta})$ in comparison with σ_{zz}^{η} in (5). Therefore, substituting (28) into (9) and using (5) give the matrix axial stress as

$$\sigma_{zz}^{m} = \sigma_{r_{ip}}^{m} + \frac{r_m^2 \ln(r/r_{ip}) - \frac{1}{2}(r^2 - r_{ip}^2)}{\left(r_m^2 \ln(r_m/r_{ip}) - \frac{1}{2}(r_m^2 - r_{ip}^2)\right)} (\sigma_{r_m}^{m} - \sigma_{r_{ip}}^{m}), \tag{29}$$

where $\sigma_{r_{ip}}^{m}$ and $\sigma_{r_m}^{m}$ are the matrix axial stresses at r_{ip} and r_m, respectively.

Similarly, $w^{ip}(r, z)$, the interphase axial displacement, can be determined by substituting (26) into (6) and (10), and integrating with respect to r from r_f to r as

$$w^{ip}(r, z) = w_{r_f}^{ip} + \frac{\left(r_{ip}^2 \ln(r/r_f) - \frac{1}{2}(r^2 - r_f^2)\right)}{G_{ip}} \left(A(w_{r_{ip}}^{ip} - w_{r_f}^{ip}) + B(w_{r_m}^{m} - w_{r_{ip}}^{m})\right)$$
$$+ \frac{C\left(\frac{1}{2}(r^2 - r_f^2) - r_f^2 \ln(r/r_f)\right)}{G_{ip}} (w_{r_m}^{m} - w_{r_{ip}}^{m}). \tag{30}$$

When E_{ip} is a constant, equation (30) reduces to the value reported by Zhang and He [2008]. Therefore, the average axial displacement of the interphase, $\overline{w^{ip}}(r, z)$, is

$$\overline{w^{ip}}(r, z) = w_{r_f}^{ip} + (w_{r_m}^{m} - w_{r_{ip}}^{m}) \frac{E_m(1 + \nu_{ip})}{E_{ip}(1 + \nu_m)} \left(\frac{\lambda_2 \lambda_4 - \lambda_1 \lambda_5}{\lambda_1 \lambda_3}\right) + \frac{\lambda_4}{\lambda_1}(w_{r_{ip}}^{ip} - w_{r_f}^{ip}), \tag{31}$$

where

$$\lambda_1 = \frac{r_{ip}^2}{r_{ip}^2 - r_f^2} \ln \frac{r_{ip}}{r_f} - \frac{1}{2}, \qquad \lambda_2 = \frac{r_f^2}{r_{ip}^2 - r_f^2} \ln \frac{r_{ip}}{r_f} - \frac{1}{2}, \qquad \lambda_3 = \frac{r_m^2}{r_m^2 - r_{ip}^2} \ln \frac{r_m}{r_{ip}} - \frac{1}{2},$$

$$\lambda_4 = \frac{r_{ip}^4 \ln(r_{ip}/r_f) - \frac{1}{4}(3r_{ip}^2 - r_f^2)(r_{ip}^2 - r_f^2)}{(r_{ip}^2 - r_f^2)^2}, \qquad \lambda_5 = \frac{r_{ip}^2 r_f^2 \ln(r_{ip}/r_f) - \frac{1}{4}(r_{ip}^4 - r_f^4)}{(r_{ip}^2 - r_f^2)^2}. \tag{32}$$

Finally, substituting (30) into (9) and using (5) give the interphase axial stress as

$$\sigma_{zz}^{ip} = \sigma_{r_f}^{ip} + \frac{\left(r_{ip}^2 \ln(r/r_f) - \frac{1}{2}(r^2 - r_f^2)\right)}{G_{ip}} \left(A(\sigma_{r_{ip}}^{ip} - \sigma_{r_f}^{ip}) + B\frac{E_{ip}}{E_m}(\sigma_{r_m}^{m} - \sigma_{r_{ip}}^{m})\right)$$
$$+ C\left(\frac{1}{2}(r^2 - r_f^2) - r_f^2 \ln(r/r_f)\right) \frac{2(1 + \nu_{ip})}{E_m} (\sigma_{r_m}^{m} - \sigma_{r_{ip}}^{m}), \tag{33}$$

where $\sigma_{r_f}^{ip}$ and $\sigma_{r_{ip}}^{ip}$ are the interphase axial stresses at r_f and r_{ip}, respectively.

2.5. *Obtaining the elastic modulus of the composite.* The effective Young's modulus of the composite, E_c, can be determined as

$$E_c = \frac{\sigma_0}{w/l_m}, \tag{34}$$

where w is the matrix axial displacement of the unit cell at $z = l_m$.

To determine w at $z = l_m$, the matrix axial displacement as a function of z must be determined. Here, using (6) and (10) and assuming that $\partial u^\eta / \partial z \ll \partial w^\eta / \partial r$ one can obtain

$$\tau_{rz}^m = G_m \frac{\partial w^m}{\partial r} \longrightarrow w^m = \frac{1}{G_m} \int \tau_{rz}^m \, dr. \tag{35}$$

Now, to determine τ_{rz}^m as a function of z, the average axial stress in the fiber and interphase as functions of z should be obtained first. Hence, substituting (24) into shear-lag equation, (18), and differentiating the resultant equation using (5) and (9) with respect to z yields

$$\frac{d^2(\overline{\sigma_{zz}^f})}{dz^2} - \lambda^2 \overline{\sigma_{zz}^f} = \alpha \overline{\sigma_{zz}^{ip}} + \beta \sigma_0. \tag{36}$$

Similarly, substituting (23) and (24) into (20) and differentiating the resultant equation with respect to z yield

$$\frac{d^2 \overline{\sigma_{zz}^{ip}}}{dz^2} - \bar{\lambda}^2 \overline{\sigma_{zz}^{ip}} = \bar{\alpha} \overline{\sigma_{zz}^f} + \bar{\beta} \sigma_0, \tag{37}$$

where

$$\alpha = -2\left(\frac{r_{ip}^2}{r_f^2} - 1\right)\left(\frac{A}{E_{ip}} - \frac{B}{E_m}\chi_1\chi_2\right), \qquad \bar{\alpha} = \frac{2(C-B)}{E_m}r_f^2\chi_1 - \frac{2A}{E_f},$$

$$\beta = -2\left(\frac{r_{ip}^2}{r_f^2} - 1\right)\frac{B}{E_m}r_m^2\chi_1, \qquad \bar{\beta} = -\frac{2(C-B)}{E_m}r_m^2\chi_1, \tag{38}$$

$$\lambda = \left[2\left(\frac{r_{ip}^2}{r_f^2} - 1\right)\left(\frac{A}{E_f} + \frac{B}{E_m}r_f^2\chi_1\right)\right]^{1/2}, \qquad \bar{\lambda} = \left(\frac{2(C-B)}{E_m}\chi_1\chi_2 + \frac{2A}{E_{ip}}\right)^{1/2},$$

in terms of the parameters

$$\chi_1 = \frac{\left(r_m^2 \ln(r_m/r_{ip}) - \frac{1}{2}(r_m^2 - r_{ip}^2)\right)}{\left(r_m^4 \ln(r_m/r_{ip}) - \frac{1}{4}(r_m^2 - r_{ip}^2)(3r_m^2 - r_{ip}^2)\right)}, \qquad \chi_2 = r_{ip}^2 - r_f^2 + \frac{E_m}{E_{ip}}(r_m^2 - r_{ip}^2). \tag{39}$$

It should be noted that when the interphase layer thickness is set to zero, i.e. $r_{ip} - r_f = 0$, substituting (24) into (18) and differentiating with respect to z reduce (36) and (37) to (40) which is the same as that of Gao and Li [2005]:

$$\frac{d^2 \overline{\sigma_{zz}^f}}{dz^2} - \lambda^2 \overline{\sigma_{zz}^f} = -\lambda^2 \frac{r_m^2}{r_f^2 + \frac{E_m}{E_f}(r_m^2 - r_f^2)}\sigma_0. \tag{40}$$

In this equation, the average axial stress in fiber $\overline{\sigma_{zz}^f}$ and interfacial shear stress τ_1 can be obtained with the same form as those given by Gao and Li [2005].

Using (36) and (37), one can obtain a fourth-order characteristic equation as

$$m^4 - (\lambda^2 + \bar{\lambda}^2)m^2 + (\lambda^2 \bar{\lambda}^2 - \alpha\bar{\alpha}) = 0. \tag{41}$$

In order to obtain the shear and axial stresses in all three phases, the roots of the characteristic equation should be obtained first. The characteristic equation has four distinct real roots for which negative values are not feasible. The positive values of the roots can be calculated as follows:

$$m_1 = \sqrt{\frac{(\lambda^2 + \bar{\lambda}^2) + \sqrt{(\lambda^2 - \bar{\lambda}^2)^2 + 4\alpha\bar{\alpha}}}{2}}, \qquad m_2 = \sqrt{\frac{(\lambda^2 + \bar{\lambda}^2) - \sqrt{(\lambda^2 - \bar{\lambda}^2)^2 + 4\alpha\bar{\alpha}}}{2}}. \tag{42}$$

Solve (36) and (37) for fiber and interphase average axial stresses:

$$\overline{\sigma_{zz}^f} = c_1 e^{m_1 z} + c_2 e^{-m_1 z} + c_3 e^{m_2 z} + c_4 e^{-m_2 z} + \frac{\bar{\beta}\alpha - \bar{\lambda}^2\beta}{\lambda^2\bar{\lambda}^2 - \alpha\bar{\alpha}} \sigma_0, \tag{43}$$

$$\overline{\sigma_{zz}^{ip}} = \frac{m_1^2 - \lambda^2}{\alpha}(c_1 e^{m_1 z} + c_2 e^{-m_1 z}) + \frac{m_2^2 - \lambda^2}{\alpha}(c_3 e^{m_2 z} + c_4 e^{-m_2 z}) - \frac{\bar{\beta}\lambda^2 - \beta\bar{\alpha}}{\lambda^2\bar{\lambda}^2 - \alpha\bar{\alpha}} \sigma_0. \tag{44}$$

Substitute (43) into (18) to obtain the shear stress at the interface between the fiber and interphase as

$$\tau_1 = -\frac{r_f}{2}\left(m_1(c_1 e^{m_1 z} - c_2 e^{-m_1 z}) + m_2(c_3 e^{m_2 z} - c_4 e^{-m_2 z})\right). \tag{45}$$

Also, substituting (44) and (45) into (20) gives the shear stress at the interface between interphase and matrix as

$$\tau_2 = -\frac{m_1}{2r_{ip}\alpha}\left((r_{ip}^2 - r_f^2)(m_1^2 - \lambda^2) + \alpha r_f^2\right)(c_1 e^{m_1 z} - c_2 e^{-m_1 z})$$
$$- \frac{m_2}{2r_{ip}\alpha}\left((r_{ip}^2 - r_f^2)(m_2^2 - \lambda^2) + \alpha r_f^2\right)(c_3 e^{m_2 z} - c_4 e^{-m_2 z}). \tag{46}$$

Next, the shear stresses in fiber, interphase, and matrix are obtained by substituting (45) and (46) into (19), (21), and (22), respectively:

$$\tau_{rz}^f(r, z) = -\frac{r}{2}\left(m_1(c_1 e^{m_1 z} - c_2 e^{-m_1 z}) + m_2(c_3 e^{m_2 z} - c_4 e^{-m_2 z})\right), \tag{47}$$

$$\tau_{rz}^{ip}(r, z) = -\frac{(c_1 e^{m_1 z} - c_2 e^{-m_1 z})}{2(r_{ip}^2 - r_f^2)\alpha}\left[m_1\left(r - \frac{r_f^2}{2}\right)((r_{ip}^2 - r_f^2)(m_1^2 - \lambda^2) + \alpha r_f^2) + m_1 r_f^2 \alpha\left(\frac{r_{ip}^2}{r} - r\right)\right]$$
$$- \frac{(c_3 e^{m_2 z} - c_4 e^{-m_2 z})}{2(r_{ip}^2 - r_f^2)\alpha}\left[m_2\left(r - \frac{r_f^2}{r}\right)((r_{ip}^2 - r_f^2)(m_2^2 - \lambda^2) + \alpha r_f^2) + m_2 r_f^2 \alpha\left(\frac{r_{ip}^2}{r} - r\right)\right], \tag{48}$$

$$\tau_{rz}^m(r, z) = -\frac{(r_m^2/r - r)}{2\alpha(r_m^2 - r_{ip}^2)}\left[m_1(c_1 e^{m_1 z} - c_2 e^{-m_1 z})\left((r_{ip}^2 - r_f^2)(m_1^2 - \lambda^2) + \alpha r_f^2\right)\right.$$
$$\left. + m_2(c_3 e^{m_2 z} - c_4 e^{-m_2 z})\left((r_{ip}^2 - r_f^2)(m_2^2 - \lambda^2) + \alpha r_f^2\right)\right]. \tag{49}$$

Because the average axial stresses of the fiber, matrix and interphase at $z = l_m$ are equal to applied stress σ_0 and interfacial shear stresses τ_1 and τ_2 are equal to zero at the center of the unit cell ($z = 0$),

Material	Young's modulus (GPa)	Poisson's ratio
Carbon nanotube	1000	0.28
Polymer matrix	2.5	0.3
Interphase	10	0.3

Table 1. Mechanical properties of the materials used in the model [Kumar and Srinivas 2014].

the constants c_1 to c_4 can be determined as

$$c_1 = c_2 = \frac{\frac{m_2^2 - \lambda^2}{\alpha}\left(1 - \frac{\bar{\beta}\alpha - \bar{\lambda}^2\beta}{\lambda^2\bar{\lambda}^2 - \alpha\bar{\alpha}}\right) - \frac{\bar{\beta}\lambda^2 - \beta\bar{\alpha}}{\lambda^2\bar{\lambda}^2 - \alpha\bar{\alpha}} - 1}{(e^{m_1 l_m} + e^{-m_1 l_m})\frac{m_2^2 - m_1^2}{\alpha}} \sigma_0, \tag{50}$$

$$c_3 = c_4 = \frac{1 - \frac{m_1^2 - \lambda^2}{\alpha}\left(1 - \frac{\bar{\beta}\alpha - \bar{\lambda}^2\beta}{\lambda^2\bar{\lambda}^2 - \alpha\bar{\alpha}}\right) + \frac{\bar{\beta}\lambda^2 - \beta\bar{\alpha}}{\lambda^2\bar{\lambda}^2 - \alpha\bar{\alpha}}}{(e^{m_2 l_m} + e^{-m_2 l_m})\frac{m_2^2 - m_1^2}{\alpha}} \sigma_0. \tag{51}$$

Finally, substituting (49) into (35) and integrating with respect to r from r_{ip} to r_m, gives the matrix axial displacement. Its value at $z = l_m$ is

$$w = \frac{r_m^2 \ln r_{ip} - r_{ip}^2/2}{2\alpha G_m(r_m^2 - r_{ip}^2)}\Big[m_1 c_1(e^{m_1 l_m} - e^{-m_1 l_m})\big((r_{ip}^2 - r_f^2)(m_1^2 - \lambda^2) + \alpha r_f^2\big)$$
$$+ m_2 c_3(e^{m_2 l_m} - e^{-m_2 l_m})\big((r_{ip}^2 - r_f^2)(m_2^2 - \lambda^2) + \alpha r_f^2\big)\Big]. \tag{52}$$

3. Results and discussion

Two case studies of composite materials having interphase regions were considered to examine the validity of the present analytical model. The composite materials were CNT-reinforced polymer composites (CNTRC) and aramid fiber reinforced rubber composites (AFRC). The results obtained using the proposed analytical modeling was compared with available experimental studies and with the results of the FE model in ABAQUS software. Moreover, the effect of the geometrical factors and mechanical properties of the constituents were investigated for each case study.

3.1. *Case study 1 (CNTRC).* In this case study, capped nanotube is replaced by a solid cylindrical fiber with flat ends [Gao and Li 2005]. The elastic modulus of CNT is $E_{\text{CNT}} = 1000\,\text{GPa}$ while the effective elastic modulus of fiber is determined as $E_f = 1006\,\text{GPa}$ [Gao and Li 2005; Ang and Ahmed 2013]. The dimensions of RVE are taken to be $r_f = 0.471\,\text{nm}$ and $r_m = 5r_f$ where r_f and r_m are the fiber and matrix radii, respectively [Gao and Li 2005]. Also, the nanotube thickness is $t_{\text{CNT}} = 0.34\,\text{nm}$ though the interphase thickness can be determined versus nanotube thickness as $t_i/t_{\text{CNT}} = 1$ [Hernández-Pérez and Avilés 2010]. Other required mechanical specifications are represented in Table 1.

3.1.1. *Analytical model validation.* The analytical results were validated by FE simulation of a full-continuum three-phase model as shown in Figure 1. The analytical and FE results of the normalized average axial stress in the fiber and matrix and normalized shear stress at the interface between the fiber and interphase versus the normalized length of the fiber are presented in Figures 2 and 3. Good
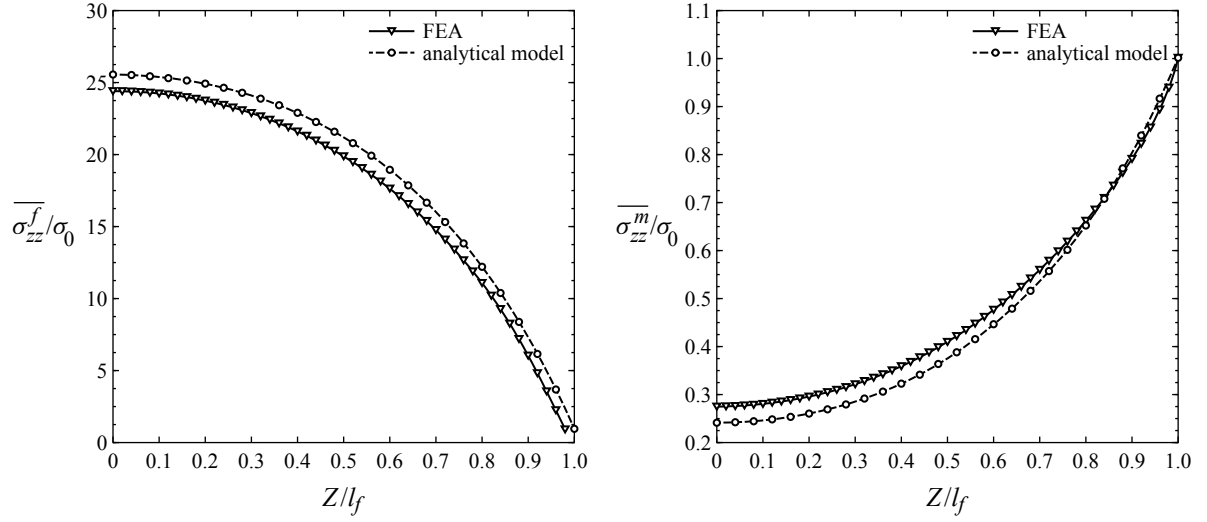
Figure 2. Analytical and FEA results of normalized average axial stress in fiber (left) and matrix (right) versus normalized fiber length.
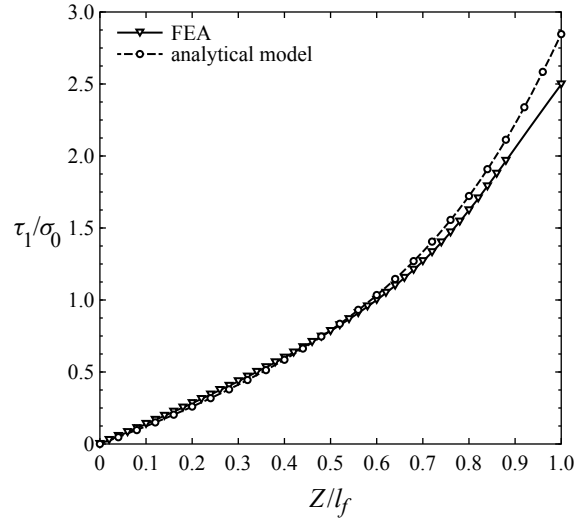
Figure 3. Analytical and FEA results of normalized shear stress at the interface between fiber and interphase versus normalized length of fiber.

agreement was found between the analytical and numerical predictions for these stress components, which demonstrates the capability of the proposed analytical model.

Validation was also done by calculating the axial elastic modulus of the composite normalized by the matrix elastic modulus and comparing it with the results presented by Hernández-Pérez and Avilés [2010]. Figure 4 shows the influence of interphase thickness on the elastic modulus of the composite. As seen, the modulus of the CNTRC strongly depends on the thickness of the interphase. The maximum
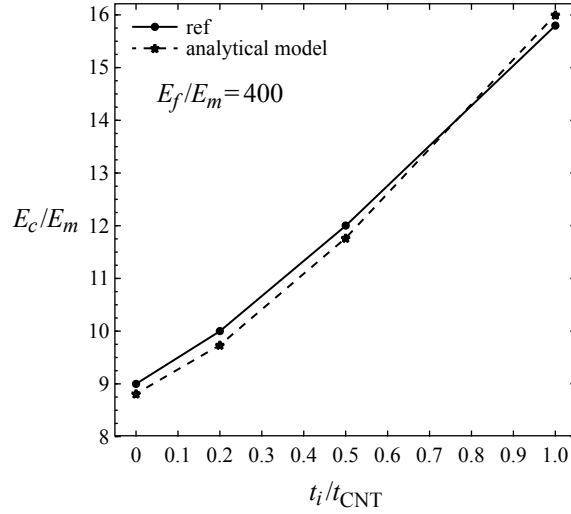
Figure 4. Axial elastic modulus of composite versus interphase thickness. The reference curve (solid) is from [Kumar and Srinivas 2014].

value for the CNTRC elastic modulus was obtained at a thickness ratio equal to one, i.e. $t_i/t_{\text{CNT}} = 1$. This result has been confirmed by other researchers [Wan et al. 2005].

Now, the influence of effective parameters such as fiber aspect ratio, matrix-to-nanotube modulus ratio and inhomogeneity of the interphase are investigated to determine the analytical modeling accuracy.

3.1.2. *Effect of fiber aspect ratio.* The average axial stresses of fiber and interphase normalized by the applied stress σ_0 in four different aspect ratios along the fiber length are presented in Figure 5.
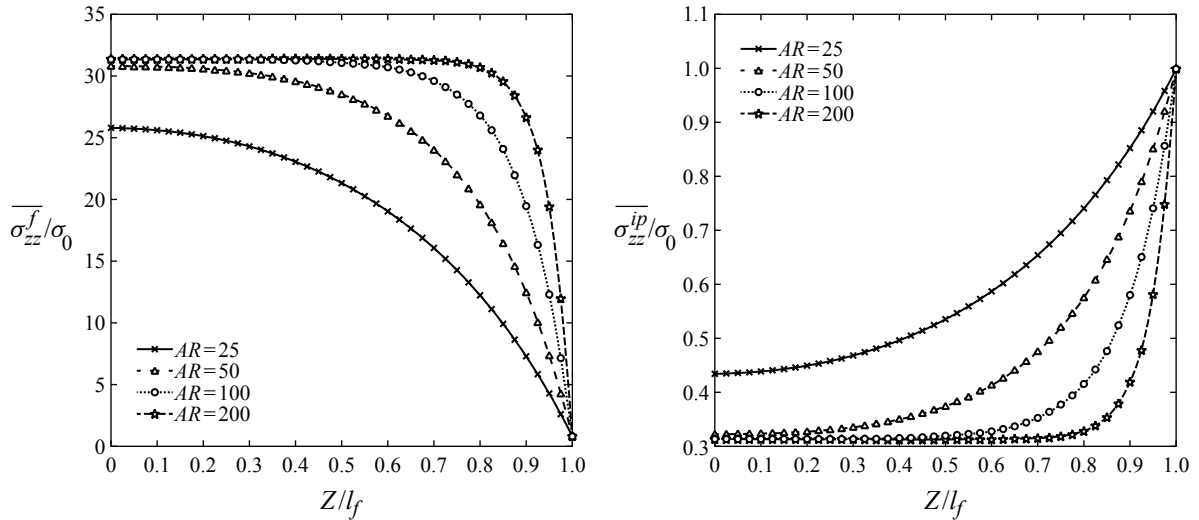
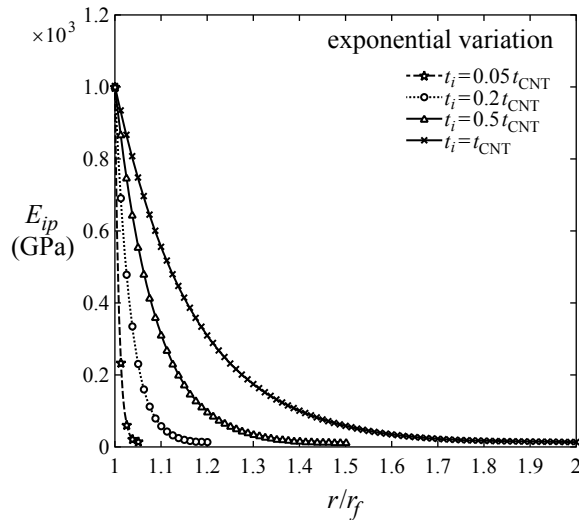**Figure 5.** Normalized axial stress in fiber (left) and in interphase (right) versus normalized length of fiber for various aspect ratios.
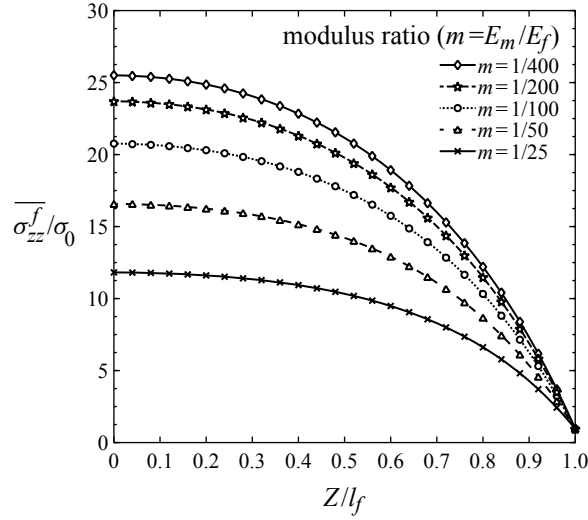
Figure 6. Normalized average axial stress of CNT along the fiber length in five different ratios of matrix to fiber elastic modulus.

As shown, the axial stress in the fiber increased as the aspect ratio increased and the axial stress in interphase decreased as aspect ratio increased. It can be concluded that more loads are transmitted to the fiber at high aspect ratios.

3.1.3. *Effects of the ratio of matrix to fiber elastic modulus.* The average axial stress of the fiber and the interfacial shear stress of the fiber-interphase along the fiber length are presented for five ratios of matrix to fiber elastic modulus, $m = E_m/E_f$. Figure 6 shows the average axial stress of the fiber normalized by applied stress σ_0 along the fiber length.

The figure shows that a decrease in the modulus ratio will increase the axial stress of the CNTs, which indicates that more loads have been transmitted to the fiber. The interfacial shear stress of the fiber-interphase normalized by applied stress σ_0 along the fiber length is shown in Figure 7.

As mentioned, based on shear-lag theory, the interfacial shear stress of fiber-interphase τ_1 increase with a decrease in the modulus ratio. Hence, the CNTs will be stronger at lower values of m and the load capacity will increase. There are no significant differences between the results of the axial and shear stresses of CNTs for values of m smaller than $1/200$. In addition, if the elastic modulus of the fiber and matrix are equal ($m \approx 1$), the axial stress of the fiber will be equal to applied stress σ_0, which suggests that reinforcement has no effect on composite strength.

3.1.4. *Effect of inhomogeneous interphase.* In order to investigate the effect of an inhomogeneous interphase on the stress transfer mechanism in a three-phase micromechanics model, the interphase Young's modulus was considered to be an exponential function of r as

$$E_{ip}(r) = P e^{-Qr}, \tag{53}$$

where P and Q are material constants obtained by applying the continuity condition of the modulus at
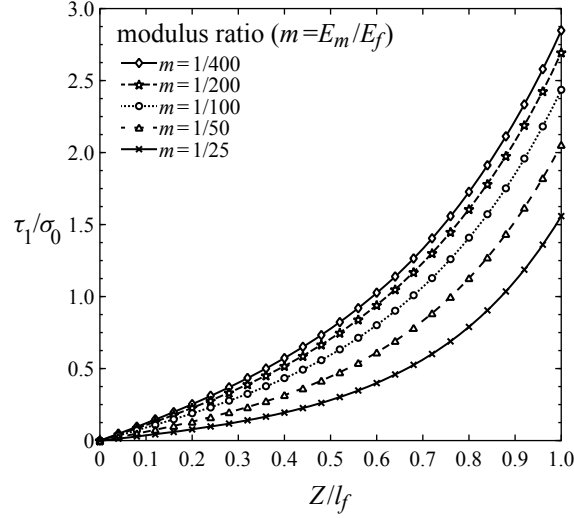
Figure 7. Normalized interfacial shear stress of fiber-interphase along the fiber length in five different ratios of matrix to fiber elastic modulus.

the interfaces:

$$Q = \frac{1}{t_1} \ln \frac{E_f}{E_m}, \qquad P = E_m e^{Q(r_f + t_i)}. \tag{54}$$

The variation in the interphase Young's modulus E_{ip} along the normalized RVE radius at four ratios of interphase thickness is shown in Figure 8. Because the Young's modulus of the fiber was considerably higher than that of the matrix, E_{ip} decreased with an increase in r from r_f to r_{ip} because of the continuity of the Young's modulus over the interfaces.

Figure 8. Interphase Young modulus (E_{ip}) along the normalized RVE radius in four different ratios of interphase thickness.
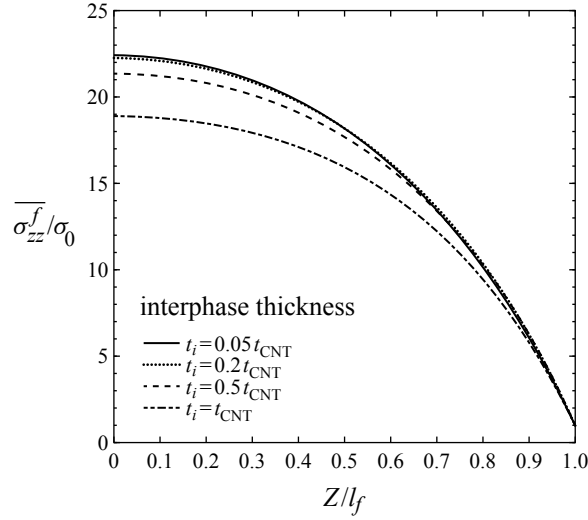
Figure 9. Normalized average axial stress of CNT along the fiber length in four different ratios of interphase thickness.

Figure 9 shows the average axial stress of CNTs normalized by applied stress σ_0 along the fiber length at four ratios of interphase thickness. As seen, the average axial stress in the fiber decreased with an increase in the interphase thickness. Consequently, the volume fraction of the interphase increased while the volume fraction of matrix decreased, which suggests that the contribution of the fiber for bearing the applied load decreased substantially.

The interfacial shear stresses of the fiber-interphase and interphase-matrix, τ_1 and τ_2, normalized by applied stress σ_0 along the fiber length at four ratios of interphase thickness are shown in Figure 10. Both interfacial shear stresses τ_1 and τ_2 increased with a decrease in the interphase thickness.

3.2. *Case study 2 (AFRC).* The material used in this case study was AFRC, the mechanical properties of which are given in Table 2.

The RVE radius was $r_m = 5r_f$ and the dimensions of the fiber were $r_f = 6\,\mu\text{m}$ and $l_f = 15r_f$ where r_f is the fiber radius and l_f is the half length of the RVE [Yu et al. 2015]. The interphase thickness varied from 0 to $1\,\mu\text{m}$, which is in accordance with the suggestions made by Papanicolaou et al. [2007]. For the composite used here, the interphase elastic modulus and Poisson's ratio were assumed to be functions of r_f as presented in (55) as suggested by Shen and Li [2003]:

$$Z_{ip}(r) = Z_m\left[1 - \frac{P}{t_i^Q}(r_{ip} - r)^Q\right]. \tag{55}$$

Material	Young's modulus	Poisson's ratio
Fiber	136 GPa	0.2
Matrix	128 MPa	0.3

Table 2. Mechanical properties of aramid fiber reinforced composite [Coffey et al. 2007].
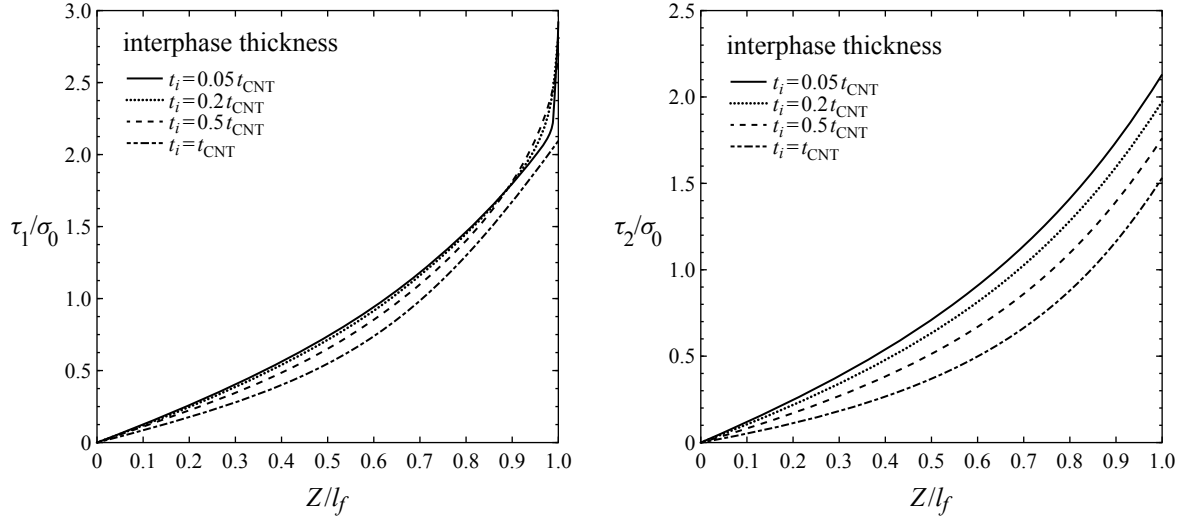
Figure 10. Normalized interfacial shear stress of fiber-interphase (left) and interphase-matrix (right) along fiber length in four different ratios of interphase thickness.

The symbol Z in (55) denotes both the elastic modulus and the Poisson's ratio. The constant Q varies from 0.2 to 3 and the constant P can be given as

$$P = \frac{Z_m - Z_{ip}(r_f)}{Z_m}. \tag{56}$$

Figure 11 shows the predicted values of the average elastic modulus and Poisson's ratio of the interphase versus Q. The Poisson's ratio increased with Q, going from 0.216 to 0.275. The average elastic modulus decreased with an increase in Q, varying from 134 GPa to 113 GPa.
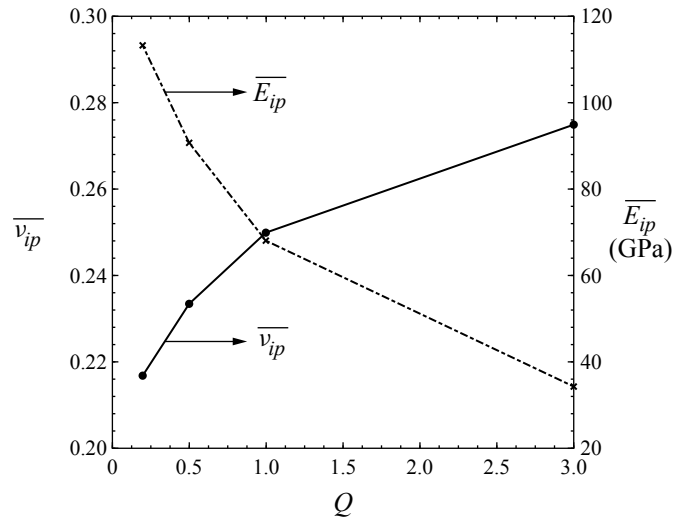
Figure 11. Average elastic modulus and Poisson's ratio of the interphase versus Q.
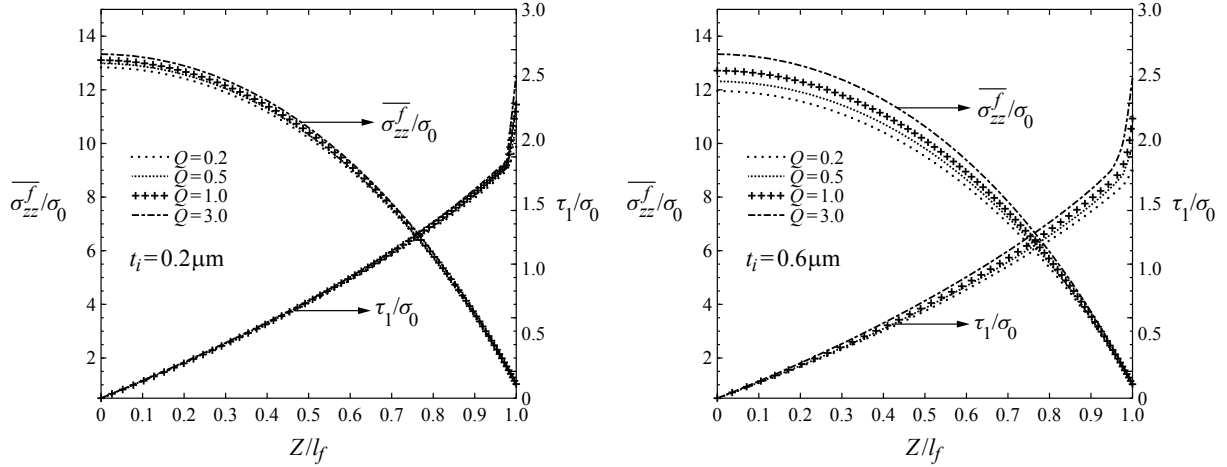
Figure 12. Average stress of fiber and interfacial shear stress of fiber-interphase along the fiber length at four different values of Q for $t_i = 0.2\,\mu$m (left) and for $t_i = 0.6\,\mu$m (right).

The normalized average stress of the fiber and the normalized interfacial shear stress of the fiber-interphase along the fiber length at four values of Q were obtained for interphase thicknesses of $t_i = 0.2\,\mu$m and $t_i = 0.6\,\mu$m as depicted in Figure 12.

As is clear from the figures, both the average axial stress of the fiber and interfacial shear stress τ_1 increased with an increase in Q because the elastic modulus of the interphase decreased with an increase in Q. Also, the dependence of the fiber axial and interfacial stresses on Q was noticeably at higher interphase thicknesses, which is in accordance with the results obtained by Kiritsi and Anifantis [2001].

Figure 13 shows the normalized average stress of the fiber and the normalized interfacial shear stress
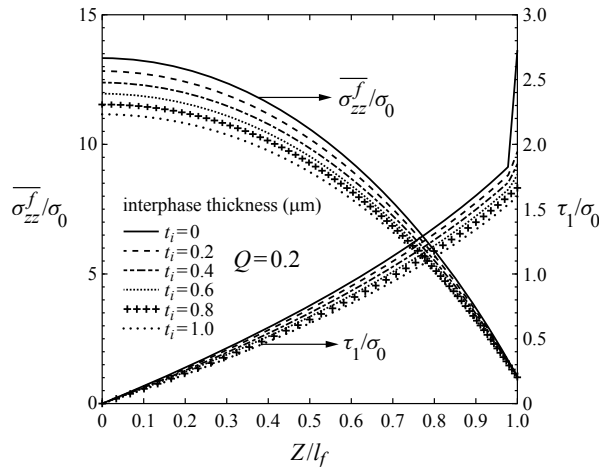
Figure 13. Average stress of fiber and interfacial shear stress of fiber-interphase along the fiber length in six different thicknesses of interphase for $Q = 0.2$.

Q	$\overline{\sigma^f_{\max}}/\sigma_0$		$\tau_{\max}/\sigma_0$	
	$v_{ip} = cte$	$v_{ip}(r)$	$v_{ip} = cte$	$v_{ip}(r)$
0.2	11.9464	11.947	1.758	1.7653
0.6	13.3192	13.3194	2.4671	2.4745

Table 3. Effect of radial dependency of interphase Poisson's ratio on the average stress of fiber and interfacial shear stress of fiber-interphase for $t_i = 0.6\,\mu$m.

of the fiber-interphase along the fiber length at $Q = 0.2$ at six interphase thicknesses from 0 to $1\,\mu$m. As seen, the stresses decreased as the interphase thickness increased; thus, at $t_i = 0$ without considering the interphase region, the average axial stress of the fiber and interfacial shear stress τ_1 reach their maximum values.

It is noted that the radial dependence for the interphase Poisson's ratio had no significant effect on the average stress of the fiber and the interfacial shear stress of the fiber-interphase. The normalized maximum average stress of the fiber and the normalized maximum interfacial shear stress of the fiber-interphase at $t_i = 0.6\,\mu$m with and without radial dependence on the interphase Poisson's ratio are given in Table 3.

As shown, radial variation of the interphase Poisson's ratio had a slight effect on the maximum average stress of the fiber and maximum interfacial shear stress of the fiber-interphase. This may be due to the fact that the difference between the Poisson's ratios of the fiber and matrix was small. Thus, the radial variation of the Poisson's ratio of the interphase can be neglected.

Finally, the analytical model was validated by comparison of the results with those obtained from available experimental measurements. Comparison of the analytical model predictions and Raman spectroscopy experimental data [Coffey et al. 2007] of the fiber axial stress obtained for applied stress
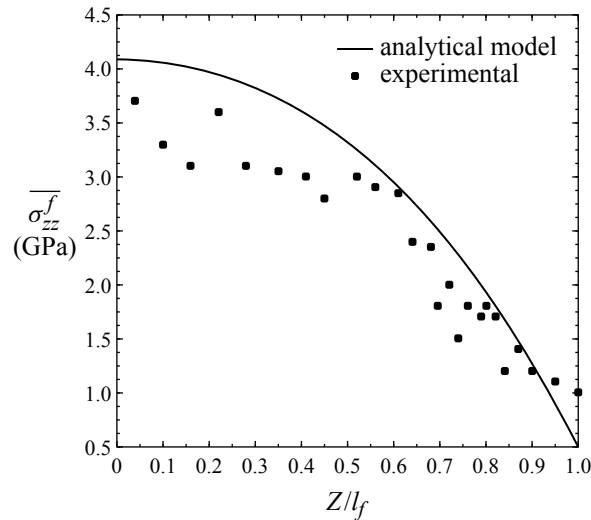
Figure 14. Comparison of analytical model prediction with experimental data of fiber axial stress for applied stress $\sigma_0 = 10\,$MPa [Coffey et al. 2007].

$\sigma_0 = 10$ MPa is shown in Figure 14. More information on the experimental measurements of the average axial stress of the fiber can be found in [Coffey et al. 2007].

Figure 14 shows that the average axial stress of the fiber is in good agreement with the experimental measurements, especially for $Z/l_f > 0.5$. Therefore, the accuracy of the proposed analytical model and the results of this research has been validated as well.

4. Conclusion

A three-phase shear-lag model was developed to investigate the effects of an inhomogeneous interphase on the mechanism of stress transfer in unidirectional fibrous composites. Considering the results of two case studies on composite materials having interphase regions, CNTRC and AFRC, the following conclusions were made.

- The thickness of the interphase strongly influenced the elastic modulus of the CNTRC, such that the maximum value of the composite elastic modulus occurred at an interphase thickness which was equal to the radius of the fiber.

- The average axial stress in fiber decreased with an increase in the interphase thickness and interfacial shear stresses τ_1 and τ_2 increased with a decrease in the interphase thickness.

- The average axial stress of the fiber and the interfacial shear stress of the fiber-interphase increased with a decrease in the modulus ratio, which indicates that the fiber was stronger at lower modulus ratios and, consequently, its load capacity increased.

- When the difference between the Poisson's ratio of the fiber and matrix was small, the radial variation of the interphase Poisson's ratio could be neglected.

- Finally, the results obtained by the proposed analytical model were in good agreement with the results of FE analysis and the available experimental measurements, which demonstrates the capability of the model.

References

[Abedian et al. 2007] A. Abedian, M. Mondali, and M. Pahlavanpour, "Basic modifications in 3D micromechanical modeling of short fiber composites with bonded and debonded fiber end", *Comput. Mater. Sci.* **40**:3 (2007), 421–433.

[Ang and Ahmed 2013] K. K. Ang and K. S. Ahmed, "An improved shear-lag model for carbon nanotube reinforced polymer composites", *Compos. B Eng.* **50** (2013), 7–14.

[Beyerlein and Landis 1999] I. J. Beyerlein and C. M. Landis, "Shear-lag model for failure simulations of unidirectional fiber composites including matrix stiffness", *Mech. Mater.* **31**:5 (1999), 331–350.

[Budiansky et al. 1986] B. Budiansky, J. W. Hutchinson, and A. G. Evans, "Matrix fracture in fiber-reinforced ceramics", *J. Mech. Phys. Solids* **34**:2 (1986), 167–189.

[Coffey et al. 2007] A. B. Coffey, C. M. O'Bradaigh, and R. J. Young, "Interfacial stress transfer in an aramid reinforced thermoplastic elastomer", *J. Mater. Sci.* **42**:19 (2007), 8053–8061.

[Cox 1952] H. L. Cox, "The elasticity and strength of paper and other fibrous materials", *Br. J. Appl. Phys.* **3**:3 (1952), 72–79.

[Dow 1963] N. Dow, "Study of stress near a discontinuity in a filament-reinforced composite metal", in *Space SciLab Missile and Space Division*, General Electric Co Tech., Report, 1963.

[Fu et al. 2008] S.-Y. Fu, X.-Q. Feng, B. Lauke, and Y.-W. Mai, "Effects of particle size, particle/matrix interface adhesion and particle loading on mechanical properties of particulate-polymer composites", *Compos. Part B-Eng.* **39**:6 (2008), 933–961.

[Gao and Li 2005] X.-L. Gao and K. Li, "A shear-lag model for carbon nanotube-reinforced polymer composites", *Int. J. Solids Struct.* **42**:5-6 (2005), 1649–1667.

[Golestanian and Shojaie 2010] H. Golestanian and M. Shojaie, "Numerical characterization of CNT-based polymer composites considering interface effects", *Comput. Mater. Sci.* **50**:2 (2010), 731–736.

[Halpin 1984] J. C. Halpin, *Primer on composite materials: analysis*, Technomic, Lancaster (PA), 1984.

[Haque and Ramasetty 2005] A. Haque and A. Ramasetty, "Theoretical study of stress transfer in carbon nanotube reinforced polymer matrix compositesj", *Compos. Struct.* **71**:1 (2005), 68–77.

[Hernández-Pérez and Avilés 2010] A. Hernández-Pérez and F. Avilés, "Modeling the influence of interphase on the elastic properties of carbon nanotube composites", *Comput. Mater. Sci.* **47**:4 (2010), 926–933.

[Hsueh 1988] C.-H. Hsueh, "Analytical evaluation of interfacial shear strength for fiber-reinforced ceramic composites", *J. Am. Ceram. Soc.* **71**:6 (1988), 490–493.

[Hsueh 1990] C.-H. Hsueh, "Interfacial debonding and fiber pull-out stresses of fiber-reinforced composites", *Mater. Sci. Eng. A* **123**:1 (1990), 1–11.

[Hsueh 1992] C.-H. Hsueh, "Interfacial debonding and fiber pull-out stresses of fiber-reinforced composites VII: improved analyses for bonded interfaces", *Mater. Sci. Eng. A* **154**:2 (1992), 125–132.

[Hsueh 1995] C.-H. Hsueh, "A modified analysis for stress transfer in fibre reinforced composites with bonded fibre ends", *J. Mater. Sci.* **30**:1 (1995), 219–224.

[Hsueh 2000] C.-H. Hsueh, "Young's modulus of unidirectional discontinuous-fibre composites", *Compos. Sci. Technol.* **60**:14 (2000), 2671–2680.

[Hsueh et al. 1997] C. H. Hsueh, R. J. Young, X. Yang, and P. F. Becher, "Stress transfer in a model composite containing a single embedded fiber", *Acta Mater.* **45**:4 (1997), 1469–1476.

[Kerans and Parthasarathy 1991] R. J. Kerans and T. A. Parthasarathy, "Theoretical analysis of the fiber pullout and pushout tests", *J. Am. Ceram. Soc.* **74**:7 (1991), 1585–1596.

[Kiritsi and Anifantis 2001] C. C. Kiritsi and N. K. Anifantis, "Load carrying characteristics of short fiber composites containing a heterogeneous interphase region", *Comput. Mater. Sci.* **20**:1 (2001), 86–97.

[Kumar and Srinivas 2014] P. Kumar and J. Srinivas, "Numerical evaluation of effective elastic properties of CNT-reinforced polymers for interphase effects", *Comput. Mater. Sci.* **88** (2014), 139–144.

[Lauke 2006] B. Lauke, "Determination of adhesion strength between a coated particle and polymer matrix", *Compos. Sci. Technol.* **66**:16 (2006), 3153–3160.

[Lawrence 1972] P. Lawrence, "Some theoretical consideration of fiber pull-out from an elastic matrix", *J. Mater. Sci.* **7**:1 (1972), 1–6.

[Liu and Chen 2003] Y. J. Liu and X. L. Chen, "Continuum models of carbon nanotube-based composites using the boundary element method", *Electron. J. Boundary Element.* **1**:2 (2003), 316–335.

[Luk and Keer 1979] V. K. Luk and L. M. Keer, "Stress analysis for an elastic half space containing an axially-loaded rigid cylindrical rod", *Int. J. Solids Struct.* **15**:10 (1979), 805–827.

[Maligno et al. 2010] A. R. Maligno, N. A. Warrior, and A. C. Long, "Effects of interphase material properties in unidirectional fibre reinforced composites", *Compos. Sci. Technol.* **70**:1 (2010), 36–44.

[Mondali and Abedian 2013] M. Mondali and A. Abedian, "An analytical model for stress analysis of short fiber composites in power law creep matrix", *Int. J. Non-Linear Mech.* **57** (2013), 39–49.

[Muki and Sternberg 1970] R. Muki and E. Sternberg, "Elastostatic load-transfer to a half-space from a partially embedded axially loaded rod", *Int. J. Solids Struct.* **6**:1 (1970), 69–90.

[Nair and Kim 1992] S. V. Nair and H. G. Kim, "Modification of the shear lag analysis for determination of elastic modulus of short-fiber (or Whisker) reinforced metal matrix composites", *J. Appl. Mech.* (*ASME*) **59**:2S (1992), 176–182.

[Nairn 1997] J. A. Nairn, "On the use of shear-lag methods for analysis of stress transfer in unidirectional composites", *Mech. Mater.* **26**:2 (1997), 63–80.

[Needleman et al. 2010] A. Needleman, T. L. Borders, L. C. Brinson, V. M. Flores, and L. S. Schadler, "Effect of an interphase region on debonding of a CNT reinforced polymer composite", *Compos. Sci. Technol.* **70**:15 (2010), 2207–2215.

[Papanicolaou et al. 2007] G. C. Papanicolaou, N. K. Anifantis, L. K. Keppas, and T. V. Kosmidou, "Stress analysis of short fiber-reinforced polymers incorporating a hybrid interphase region", *Compos. Interface.* **14**:2 (2007), 131–152.

[Rafiee and Pourazizi 2015] R. Rafiee and R. Pourazizi, "Influence of CNT functionalization on the interphase region between CNT and polymer", *Comput. Mater. Sci.* **96** (2015), 573–578.

[Rosen 1964] B. W. Rosen, "Tensile failure of fibrous composites", *AIAA J.* **2**:11 (1964), 1985–1991.

[Shen and Li 2003] L. Shen and J. Li, "Effective elastic moduli of composites reinforced by particle or fiber with an inhomogeneous interphase", *Int. J. Solids Struct.* **40**:6 (2003), 1393–1409.

[Takaku and Arridge 1973] A. Takaku and R. G. C. Arridge, "The effect of interfacial radial and shear stress on fiber pull-out in composite materials", *J. Phys. D* **6**:17 (1973), 2038–2047.

[Taya and Arsenault 1987] M. Taya and R. J. Arsenault, "A comparison between a shear-lag type model and an Eshelby type model in predicting the mechanical properties of a short fiber composite", *Scr. Metall.* **21**:3 (1987), 349–354.

[Timoshenko and Goodier 1970] S. P. Timoshenko and J. N. Goodier, *Theory of elasticity*, 3rd ed. ed., McGraw-Hill, New York, 1970.

[Wan et al. 2005] H. Wan, F. Delale, and L. Shen, "Effect of CNT length and CNT-matrix interphase in carbon nanotube (CNT) reinforced composites", *Mech. Res. Commun.* **32**:5 (2005), 481–489.

[Wang et al. 2006] J. Wang, S. L. Crouch, and S. G. Mogilevskaya, "Numerical modeling of the elastic behavior of fiber-reinforced composites with inhomogeneous interphases", *Compos. Sci. Technol.* **66**:1 (2006), 1–18.

[Wang et al. 2011] X. Wang, J. Zhang, Z. Wang, S. Zhou, and X. Sun, "Effects of interphase properties in unidirectional fiber reinforced composite materials", *Mater. Des.* **32**:6 (2011), 3486–3492.

[Withers et al. 1989] P. J. Withers, W. M. Stobbs, and O. B. Pederson, "The application of the eshelby method of internal stress determination to short fibre metal matrix composites", *Acta Metall.* **37**:11 (1989), 3061–3084.

[Yang and Pitchumani 2004] F. Yang and R. Pitchumani, "Effects of interphase formation on the modulus and stress concentration factor of fiber-reinforced thermosetting-matrix composites", *Compos. Sci. Technol.* **64**:10-11 (2004), 1437–1452.

[Yao et al. 2013] Y. Yao, S. Chen, and P. Chen, "The effect of a graded interphase on the mechanism of stress transfer in a fiber-reinforced composite", *Mech. Mater.* **58** (2013), 35–54.

[Yu et al. 2015] X. Yu, B. Gu, and B. Zhang, "Effects of short fiber tip geometry and inhomogeneous interphase on the stress distribution of rubber matrix sealing composites", *J. Appl. Polym. Sci.* **132**:1-8 (2015), 41638.

[Zhang and He 2008] J. Zhang and C. He, "A three-phase cylindrical shear-lag model for carbon nanotube composites", *Acta Mech.* **196**:1-2 (2008), 33–54.

[Zhang et al. 2017] B. Zhang, X. Yu, and B. Gu, "An improved shear lag model for predicting stress distribution in hybrid fiber reinforced rubber composites", *Fiber. Polym.* **18**:2 (2017), 349–356.

[Zhao and Ji 1997] P. Zhao and S. Ji, "Refinements of the shear-lag model and its applications", *Tectonophys.* **279**:1-4 (1997), 37–53.

MOHAMMAD HASSAN ZARE: zare_mhz@yahoo.com
Department of Mechanical Engineering, Science and Research Branch, Islamic Azad University, Tehran, Iran

MEHDI MONDALI: mondali@srbiau.ac.ir
Department of Mechanical Engineering, Science and Research Branch, Islamic Azad University, Tehran, Iran

JOURNAL OF MECHANICS OF MATERIALS AND STRUCTURES

msp.org/jomms

Founded by Charles R. Steele and Marie-Louise Steele

Cover photo: Ev Shafrir

Journal of Mechanics of Materials and Structures